

## Coalescence of Sessile Aqueous Droplets Laden with Surfactant

Soheil Arbabi\*,<sup>1</sup> Piotr Deuar,<sup>1</sup> Rachid Bennacer,<sup>2</sup> Zhizhao Che,<sup>3</sup> and Panagiotis E. Theodorakis\*<sup>1</sup>

<sup>1</sup>*Institute of Physics, Polish Academy of Sciences, Al. Lotników 32/46, 02-668 Warsaw, Poland*

<sup>2</sup>*Université Paris-Saclay, ENS Paris-Saclay, CNRS, LMPS, 4 Av. des Sciences, 91190 Gif-sur-Yvette, France*

<sup>3</sup>*State Key Laboratory of Engines, Tianjin University, 300350 Tianjin, China*

(\*Electronic mail: panos@ifpan.edu.pl)

(\*Electronic mail: arbabi@ifpan.edu.pl)

(Dated: 19 March 2024)

With most of the focus to date having been on the coalescence of freely suspended droplets, much less is known about the coalescence of sessile droplets, especially in the case of droplets laden with surfactant. Here, we employ large-scale molecular dynamics simulations to investigate this phenomenon on substrates with different wettability. In particular, we unravel the mass transport mechanism of surfactant during coalescence, thus explaining the key mechanisms present in the process. Close similarities are found between the coalescence of sessile droplets with equilibrium contact angles above  $90^\circ$  and that of freely suspended droplets, being practically the same when the contact angle of the sessile droplets is above  $140^\circ$ . Here, the initial contact point is an area that creates an initial contact film of surfactant that proceeds to break into engulfed aggregates. A major change in the physics appears below the  $90^\circ$  contact angle, when the initial contact point becomes small and line-like, strongly affecting many aspects of the process and allowing water to take part in the coalescence from the beginning. We find growth exponents consistent with a  $2/3$  power law on strongly wettable substrates but no evidence of linear growth. Overall bridge growth speed increases with wettability for all surfactant concentrations, but the speeding up effect becomes weaker as surfactant concentration grows, along with a general slowdown of the coalescence compared to pure water. Concurrently the duration of the initial thermally limited regime increases strongly by almost an order of magnitude for strongly wettable substrates.

## I. INTRODUCTION

Many natural phenomena involve the coalescence of fluid droplets.<sup>1–20</sup> For example, this is a fundamental process that determines the distribution and coalescence rate of raindrops in atmospheric aerosols.<sup>21–24</sup> Apart from such natural processes, droplet coalescence is relevant for many industrial applications as well, such as inkjet printing,<sup>25</sup> microfluidics,<sup>26–29</sup> and water treatment during crude oil and natural gas separation.<sup>30,31</sup> Further control of the process may involve the use of various additives,<sup>32–39</sup> such as surfactant,<sup>40–58</sup> which can reduce surface tension at fluid interfaces, crucial in multi-phase systems. For example, surfactant can stabilize droplets' surface or prevent their coalescence, thus improving the bio-compatibility in certain systems<sup>59</sup> or affecting the fusion, mixing, and manipulation of droplets in microfluidic devices.<sup>60</sup> While many efforts have thus far been taken to understand coalescence phenomena at a fundamental level,<sup>1,3,61</sup> there are still numerous aspects of this process that require further investigations, such as the coalescence of sessile droplets with surfactant.

In experiments,<sup>62–68</sup> droplet coalescence has been studied for various conditions (*e.g.*, in the presence of applied electric fields) and geometries (*e.g.*, micro-channels, fibers, *etc.*), mainly by means of high-speed imaging and electrical sensing. Due to resolution limitations, the focus of these investigations has mainly been placed on unveiling macroscopic properties of the process.<sup>49,50,52,69–71</sup> For example, the effect of surfactant concentration on droplet coalescence has been investigated by high-speed imaging.<sup>50</sup> When an asymmetry in surfactant concentration of the coalescing droplets is present, Marangoni flow was observed and the curvature on either side of the growing bridge was different. Numerical continuum approaches have also been employed to complement understanding of droplet coalescence.<sup>5,7,15,17,42,69,72–78</sup> However, such methods suffer from inadequate resolution in capturing the mass transport mechanism of surfactant during coalescence or resolving the initial contact of the droplets. The singularity at the contact point still remains a challenge for continuum simulation.<sup>7</sup> On the other hand, molecular dynamics (MD) simulation can naturally resolve the contact region at the molecular level, to observe the start of the coalescence process.

In general, droplet coalescence is a non-equilibrium process that occurs in three stages. The first stage involves the initial approach of droplets, when they come close enough to interact (pinching/contact) and form the so-called bridge (Figure 1a, e and pinching b, f). This is followed by a bridge-growth stage that leads to the reshaping (third stage) of the droplets (Figure 1c, g) and

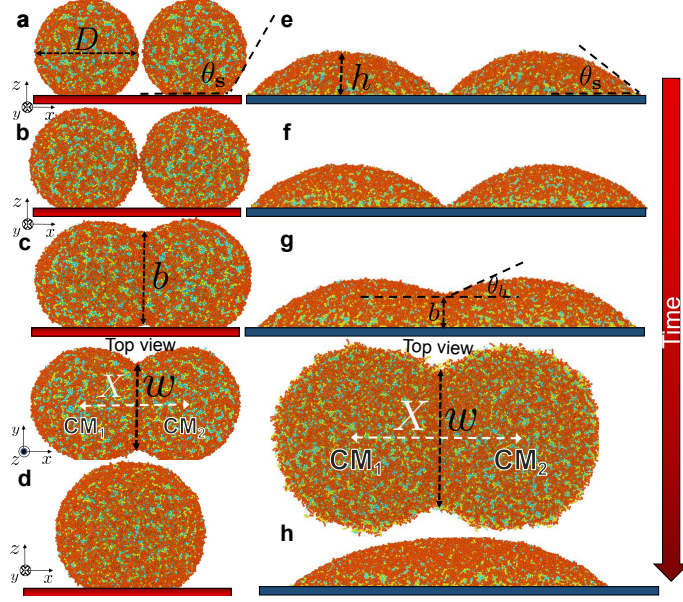


FIG. 1. Different stages of coalescence of surfactant-laden droplets on non-wettable (a–d,  $\theta_s \simeq 142^\circ$ ) and wettable (e–h,  $\theta_s \simeq 49^\circ$ ) substrates, with surfactant concentration above CAC (35.48 wt%).  $b$  is the bridge height and  $w$  the bridge width.  $X$  is distance between the centers of mass of the two droplets in the  $x$ -direction, while  $\theta_s$  is the equilibrium contact angle of the droplet.  $\theta_b$  is the angle formed at the bridge at the liquid–gas surface. The stages of coalescence shown here are: (a, e) Initial approach ( $t = t_c$ ); (b, f) Moment of pinching ( $t = t_c$ ); (c) Developed bridge ( $t = t_c + 196.25 \tau$ ) and (d) final, equilibrium state of the system ( $t = t_c + 1483.75$ ) in the case of the non-wettable substrate. (g) Developed bridge ( $t = t_c + 1028.75 \tau$ ) and (h) final, equilibrium state of the system ( $t = t_c + 3161.25 \tau$ ) in the case of the wettable substrate. The snapshots of the system were obtained using Ovito software.<sup>79</sup>

eventually the single spherical-cap shape for sessile droplets, which is the final equilibrium and minimum energy state of the system (Figure 1d,h). The time evolution of this process on substrates with different wettability is illustrated in Figure 2 (Multimedia view). The coalescence process is governed by the interplay of viscous, inertial and surface-tension forces, as the system tries to decrease the surface tension.<sup>80</sup> In particular, from the perspective of fluid dynamics, viscous forces are expected to play an important role in the initial bridge growth, which is driven primarily by molecular interactions. At a later stage of the bridge growth, inertial effects are expected to take over. In the case of freely suspended droplets, a linear scaling of the bridge radius,  $b$ , in time ( $b \propto t$ ) and logarithmic corrections  $b \propto t \ln t$  have been suggested for the viscous regime.<sup>6,81</sup> For the inertial regime, a power law scaling ( $b \propto t^{1/2}$ ) has been proposed.<sup>5</sup> However, this classification

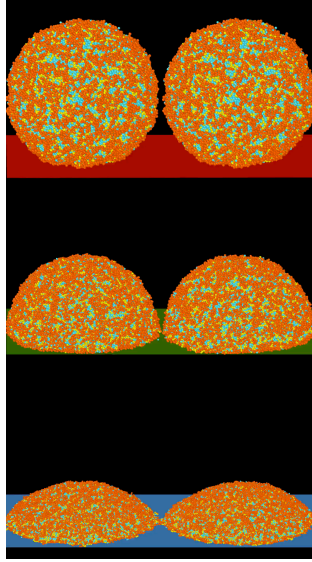


FIG. 2. (Multimedia view) Coalescence of droplets with surfactant concentration (35.48 wt%) on substrates with different wettability (upper row, non-wettable; middle row, intermediate; lower row, wettable).

is still under debate in the literature, and an inertially limited viscous (ILV) regime has also been reported.<sup>1,82</sup> Moreover, an initial thermal regime, which is inaccessible to experiments has been identified by means of all-atom<sup>4</sup> and coarse-grained (CG)<sup>83,84</sup> MD simulation. This regime arises due to collective thermal motion of particles at the droplets' surface. Here, all-atom simulation has proposed a scaling law for a length scale characterizing the extent of the thermal fluctuations, namely  $l_T \approx (k_B T / \gamma)^{1/4} R^{1/2}$ , where  $k_B$  is Boltzmann's constant,  $T$  the temperature,  $\gamma$  the surface tension, and  $R$  the droplet radius.<sup>4</sup> When the bridge radius is smaller than this length scale ( $b < l_T$ ), the bridge grows mainly due to thermal motion of particles, while later ( $b > l_T$ ) hydrodynamic effects are expected to dominate. Recent MD simulations of a CG model have indicated the presence of the thermal regime and subsequent inertial scaling law ( $b \propto t^{1/2}$ ) for the bridge growth for both aqueous droplets with and without surfactant.<sup>83,84</sup>

In the case of the coalescence of sessile droplets,<sup>34,45,81,85–91</sup> for water droplets on non-wettable substrates (contact angle  $\theta_s \geq 90^\circ$ , Figure 1) it has been suggested that the bridge grows with time as  $b \propto t^{1/2}$ , as has been observed in the case of freely suspended droplets. In contrast, for wettable substrates, namely  $\theta_s < 90^\circ$ , the bridge is predicted to grow with a new power law  $b \propto t^{2/3}$ .<sup>86</sup> Moreover, experiments of droplets with an equilibrium contact angle in the range  $10^\circ - 56^\circ$  suggest that the bridge height roughly grows in time with power-law exponents between 0.50 and 0.86. Data was seen to follow the scaling law for the entire range of time in the case of  $10^\circ$  contact angle,

while the rest of the cases studied deviated from this law at longer times.<sup>66</sup> The bulk fluid properties also affect the bridge growth. For example, in the case of polymer droplets<sup>34,92,93</sup>, their viscosity can result in a lower rate of coalescence in comparison with water droplets. One finds power-law exponents lower than 1/2 for nonwetable substrates (equilibrium contact angle greater than 90°) and power-law exponents lower than 2/3 for wettable substrates.<sup>34</sup> The bridge width,  $w$  (Figure 1), grows as  $w \propto t^{0.5}$ .<sup>66,87,88</sup> However, a linear scaling  $w \propto t$  has also been suggested for droplets of high viscosity.<sup>81</sup> To our knowledge, the regimes of applicability of the above findings have not been investigated in experiments nor in modeling that would include the early-time molecular level physics.

In view of the many unknowns in the coalescence of sessile surfactant-laden droplets, we embarked on investigating this phenomenon by using large-scale molecular dynamics simulations of a coarse-grained force-field, considering a comprehensive range of possible scenarios. Hence, our study includes a range of surfactant concentrations below and above the critical aggregation concentration (CAC) and substrates with different wettability, both wettable ( $\theta_s < 90^\circ$ ) non-wettable ( $\theta_s > 90^\circ$ ), and those with equilibrium contact angle of about 90°. In all these cases, we have explored the mass transport mechanism of surfactant, which provides insights into the details of the coalescence process, analyzed the dynamics of the bridge growth, which characterizes the rate of coalescence, as well as studied the bridge angle and the velocity of approach.<sup>94</sup> It turns out that while the coalescence of sessile surfactant-laden droplets on non-wettable substrates shares similarities with the coalescence of freely suspended droplets, significant differences in the mass transport mechanism and rate of coalescence appear for wettable substrates. The following section presents our MD simulation model and methods. Our results are discussed in Section III. Finally, the conclusions and possible suggestions for follow-up research are discussed in Section IV.

## II. SIMULATION MODEL AND METHODS

Our system consists initially of two droplets placed close to each other as shown in Figure 1a,e, that is a distance below the cutoff range of the interactions between beads in order to initiate the coalescence of the droplets. We have considered concentrations above and below the CAC for C10E4 surfactants. The details of the model for the interactions between the different components and the validation for various surfactants are taken the same here as used in a number of previous related studies,<sup>95–101</sup> and were obtained through the Mie- $\gamma$  Statistical Associating Fluid Theory

(SAFT Mie- $\gamma$ ).<sup>98,102–105</sup> The MD simulations were carried out in the canonical ensemble with the Nosé–Hoover thermostat as implemented in LAMMPS software.<sup>106,107</sup> After equilibration of a single droplet on the specific substrate, it was cloned to produce the second droplet and the surrounding vapor for the start of the coalescence *in silico* experiment (Figures 1a,e).

The force-field has been validated for a range of water–surfactant systems with a focus on reproducing key properties, such as surface tension and phase behavior.<sup>95–97,99–101,108,109</sup> In particular, interactions between the various CG beads representing different chemical units of the system are described via the Mie potential

$$U(r_{ij}) = C\varepsilon_{ij} \left[ \left( \frac{\sigma_{ij}}{r_{ij}} \right)^{\lambda_{ij}^r} - \left( \frac{\sigma_{ij}}{r_{ij}} \right)^{\lambda_{ij}^a} \right], \text{ for } r_{ij} \leq r_c, \quad (1)$$

where

$$C = \left( \frac{\lambda_{ij}^r}{\lambda_{ij}^r - \lambda_{ij}^a} \right) \left( \frac{\lambda_{ij}^r}{\lambda_{ij}^a} \right)^{\frac{\lambda_{ij}^a}{\lambda_{ij}^r - \lambda_{ij}^a}},$$

and  $i$  and  $j$  represent the bead types. Hence,  $\sigma_{ij}$  is an effective size of these beads, while  $\varepsilon_{ij}$  sets the interaction strength between beads of type  $i$  and  $j$ . One takes  $\lambda_{ij}^a = 6$ , which is connected to representing the dispersive interactions between the different particles, while  $\lambda_{ij}^r$  serves as a fitting parameter in the SAFT model and can vary. Finally,  $r_{ij}$  is the distance between any pair of beads, which interact when their distance is below a cutoff value set to  $r_c = 4.583 \sigma$ , where  $\sigma$  is the overall unit of length. The rest of the units are  $\varepsilon$  for the energy,  $m$  for the mass, while  $\tau$  is the natural MD time unit  $\tau = \sigma(m/\varepsilon)^{0.5}$ . In real units, we consider the simulation to correspond to:  $\sigma = 0.43635$  nm,  $\varepsilon/k_B = 492$  K,  $m = 44.0521$  amu and  $\tau = 1.4062$  ps. The integration of the equations of motion was carried out with an integration time-step  $\delta t = 0.005 \tau$ , while the temperature was set to  $k_B T/\varepsilon = 0.6057$ , which would correspond to  $T = 25$  °C in real units.

Here, we have chosen for our investigations the C10E4 surfactant, which has also been previously studied in the context of the coalescence of freely suspended droplets<sup>83,84</sup> and superspreading.<sup>95–97</sup> The above studies found other CmEn type surfactants to give similar behavior,<sup>83,84</sup> so here we only consider C10E4 as representative of the whole family. Then, the CG representation of the C10E4 (Figure 3) uses hydrophobic alkane CG ‘C’ beads with each one representing a  $-\text{CH}_2 - \text{CH}_2 - \text{CH}_2 -$  group of atoms. Hydrophilic CG ‘EO’ beads represent oxyethylene groups  $-\text{CH}_2 - \text{O} - \text{CH}_2$ . Finally, water CG ‘W’ beads correspond to two water molecules. The values of the nonbonded interaction parameters between CG beads are reported in Table S1 of the Supplementary Material (SM) and their masses in Table S2 of the SM.

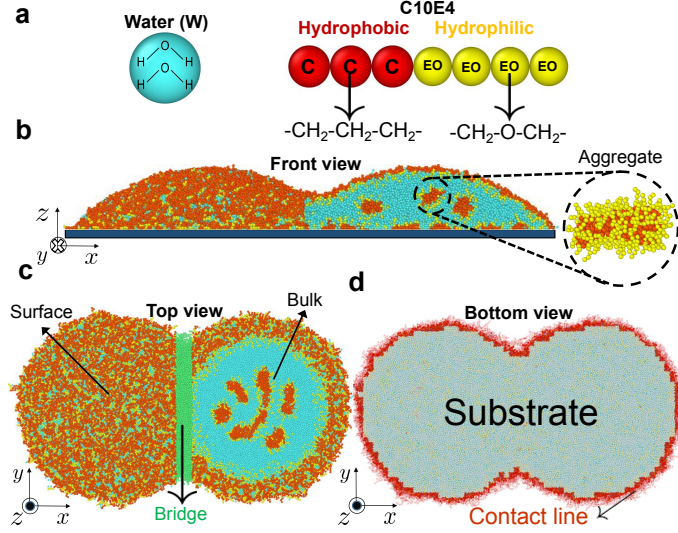


FIG. 3. Description of model and notation. (a) Coarse-grained representation of water and C10E4 surfactant. (b–d) External and cross-section views are shown to highlight the bulk, interfaces, and contact line of the droplet ( $\theta_s = 49^\circ$ , with concentration above CAC). Surrounding water vapor is omitted for the sake of clarity. (b) Front view; (c) Top view; (d) Bottom view.

To link the alkane and oxyethylene beads together, each consecutive pair of beads along the surfactant chain interacts via a harmonic potential of the form

$$V(r_{ij}) = 0.5k(r_{ij} - \sigma_{ij})^2 \quad (2)$$

where  $k = 295.33 \epsilon/\sigma^2$ . In addition, each consecutive triad of EO beads along the chain experiences a harmonic angle potential, *i.e.*

$$V_\theta(\theta_{ijk}) = 0.5k_\theta(\theta_{ijk} - \theta_0)^2 \quad (3)$$

where  $\theta_{ijk}$  is the angle between consecutive beads  $i$ ,  $j=i+1$  and  $k=j+1$ . Constants are  $k_\theta = 4.32 \epsilon/\text{rad}^2$ , and  $\theta_0 = 2.75 \text{ rad}$  for the equilibrium angle.

The total number of beads per initial droplet in each simulation was  $10^5$  and two different surfactant concentrations were considered, namely 6.25 wt%, which is below CAC, and 35.48 wt%, which is well above, with CAC roughly being 7.5 wt%.<sup>83,84</sup> The latter concentration is taken as an average, since the number of water molecules in the liquid phase (droplet) fluctuates. The wettability of the smooth, unstructured substrate was also tuned, as described below, covering a range of wettable ( $\theta_s < 90^\circ$ ) and non-wettable ( $\theta_s > 90^\circ$ ) types of substrate (Figure 1). The exact values of the equilibrium contact angle of single droplets are reported in Table S3 of the SM along with the



corresponding droplet dimensions (Table S4 of the SM). Finally, to determine the beads belonging to the liquid phase (droplet), a cluster analysis has been performed.<sup>110,111</sup>

To vary the wettability of the substrate, we need to define the interactions between the droplet beads and the substrate. This can be done by using the combining rules defined in SAFT $\gamma$ -Mie<sup>103</sup>:

$$\sigma_{ij} = \frac{\sigma_{ii} + \sigma_{jj}}{2}, \quad (4)$$

$$\epsilon_{ij} = \frac{\sqrt{\sigma_{ii}^3 \sigma_{jj}^3}}{\sigma_{ij}^3} \sqrt{\epsilon_{ii} \epsilon_{jj}}. \quad (5)$$

and start from the defined interactions for the liquid phases as given in Table S1 of the SM. By tuning the cross interaction  $\epsilon_{ws}$  (“s” indicates the substrate), the empirical relationship between  $\epsilon_{ws}$  and the contact angle of pure water droplets (Figure S1 of the SM) can be found, and is shown in Figure S2 of the SM. Then, by using the above combining rules, the parameter  $\epsilon_{ss}$  corresponding to a given  $\epsilon_{ws}$  can be obtained. We shall note here that the exact value of the  $\sigma_{ss}$  parameter is not important for our studies and is set to unity for simplicity. Similarly,  $\lambda_{sj}^r = 9$  is set for all interactions involving the substrate. Based on the knowledge of the latter parameters and the interactions  $\sigma_{ww}$  and  $\epsilon_{ww}$  (Table S1 of the SM), the interaction of the substrate with the surfactant beads can be obtained as well, again using Equations 4-5. After obtaining all the interaction parameters, equilibrium simulations are run and the surfactant-laden droplet’s contact angle is determined by using the method of Ref. 96 (see also text and Figure S1 of the SM) with data reported in Table S3 of the SM. It might be argued however that estimating the angles can in general be sensitive to the details of the definition of a sharp interface, as well as to the fitting procedure.<sup>91,112</sup> Also, models that could take into account the disjoining pressure effects, very relevant in the context of droplets on solids substrates, might perform better than fitting spherical caps to nanodroplets.<sup>91</sup> Moreover, according to a previous study,<sup>96</sup> the size of the droplet is large enough to guarantee that the equilibrium contact angle does not depend on the size of the droplet, which makes the interaction values valid for both larger and smaller droplets. Table S3 of the SM provides the exact values for all of the cross interactions between the beads and the substrate used in the simulations. Our choice here covers the relevant parameter space for surfactant concentration (above and below CAC) and substrate types (wetable, non-wetable, and about 90°).

The mass transport of surfactant molecules is investigated by tracking the motion of each individual molecule between the various parts of the droplet, which are illustrated in Figures 3c-d.

These different parts are the liquid–gas (LG) surface for the left and right droplets (the center of the coordinate system is taken to be in the middle between the two droplets where the bridge forms), the bulk of the left and right droplets, the solid–liquid (SL) interface for the left and right droplets, the contact line for the left and right droplets, and the LG and SL interfaces, bulk, and contact line of the bridge as shown in Figure 3. Hence, this makes a total of twelve different regions where each surfactant molecule can belong. Further discussion and details on the calculation of the probabilities related to the motion of surfactant between these regions describing the mass transport mechanism of surfactants can be found in the SM. Finally, we have calculated the density profiles of the water and surfactant during coalescence, and the approach distance and velocity of the droplets<sup>34</sup>, which will be further discussed in the following section.

### III. RESULTS AND DISCUSSION

#### A. Surfactant mass transport mechanism

Our previous studies<sup>83,84</sup> of the coalescence of freely suspended droplets have shown that surfactant plays an ever increasing role at the pinching point as its concentration in the droplets increases, while water has a smaller effect in initiating the coalescence process. Similar behavior is also observed in the case of  $\theta_s > 90^\circ$  shown in Figure 4 for sessile droplets, since the bridge

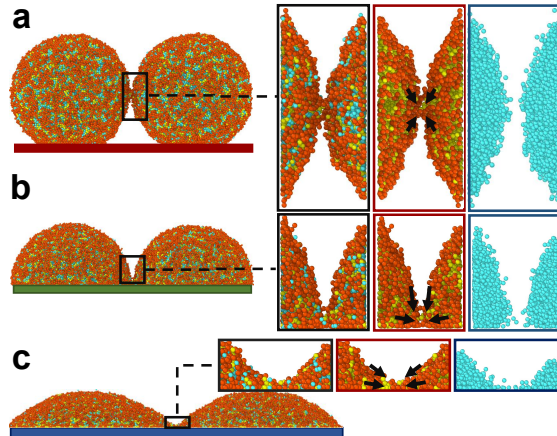


FIG. 4. The pinching moment ( $t \approx t_c$ ) in the case of (a) a non-wettable substrate ( $\theta_s > 90^\circ$ ), (b) an intermediate case ( $\theta_s \approx 90^\circ$ ), and (c) a wettable substrate ( $\theta_s < 90^\circ$ ). Water participation in the coalescence process is more pronounced in the case  $\theta_s < 90^\circ$ , while the cases  $\theta_s \geq 90^\circ$  behave very similarly to freely suspended droplets.<sup>83,84</sup> Snapshots were obtained using Ovito software.<sup>79</sup>

formation starts far from the substrate (Figure 4a). For this reason, the bridge region initially is not affected by the presence of the substrate and the bridge angle is very steep ( $\theta_b \approx 80^\circ$ , for example, see Figure S6 of the SM) when pinching occurs. For the same reason, we find that the growth of the bridge occurs symmetrically in both the  $y$  and  $z$  directions ( $b$ ,  $w$ , Figure 1). In contrast, in the case of wettable substrates, water molecules participate in the pinching process from its onset (Figure 4c).

To quantify mass transport, we count the surfactant molecule movements between the 12 regions identified in Figure 3. The raw numbers are reported in Table S5 of the SM. These set the intensity of the arrows in Figure 5, indicating the dominant direction of surfactant transport. Figures 5a–c present the dominant surfactant transport processes for the case  $\theta_s > 90^\circ$ . As in the case of freely suspended droplets, an interface film of surfactant initially forms consisting of surfactant from the LG surfaces of the droplets that come into contact. Figure 6 (Multimedia view) illustrates this in the case of non-wettable substrates, as well as the absence of this film when coalescence takes place on wettable substrates. The perimeter of the bridge is expected to linearly grow with  $b$ , while the area of the film increases as  $b^2$ . Moreover, the data in Table S5 of the SM shows that the dominant movement of surfactant is towards the LG surface of the droplets, as in the case of freely suspended droplets. Since this movement towards the LG surface occurs and the area of contact between the droplet grows, the surfactant concentration in the film decreases, the film ruptures and some surfactant remains in the form of aggregates. Due to the lack of space at the LG interface of the merged droplets, surfactant from the newly formed aggregates in the bridge bulk cannot be accommodated at the LG interface. Also, we observe surfactant transport away from the bridge from the SL interface toward the LG surface through the contact line. Other transport processes away from the bridge are insignificant during coalescence in the case of non-wettable droplets. When the contact angle  $\theta_s \approx 90^\circ$ , the pinching is similar to the case of droplets with contact angle  $\theta_s > 90^\circ$  (Figure 4) as well as the case of freely suspended droplets.<sup>83,84</sup> Finally,  $\theta_b$  has a value of around  $90^\circ$  at the pinching moment (for example, see Figure S6 of the SM).

The case  $\theta_s < 90^\circ$  shows a somewhat different behavior. The transport toward the LG surface is higher than in the cases where  $\theta_s \geq 90^\circ$ , and unlike the previous cases, we do not see the formation of new aggregates as coalescence takes place [Figure 6 (Multimedia view)]. This can be attributed to several causes. Firstly, the amount of surfactant at the bridge is smaller in the case of  $\theta_s < 90^\circ$ , due to the higher curvature of the droplets. In this case, there is only a small portion of the droplet surfaces that come into contact, at the contact line of the droplets. In contrast, for non-wettable

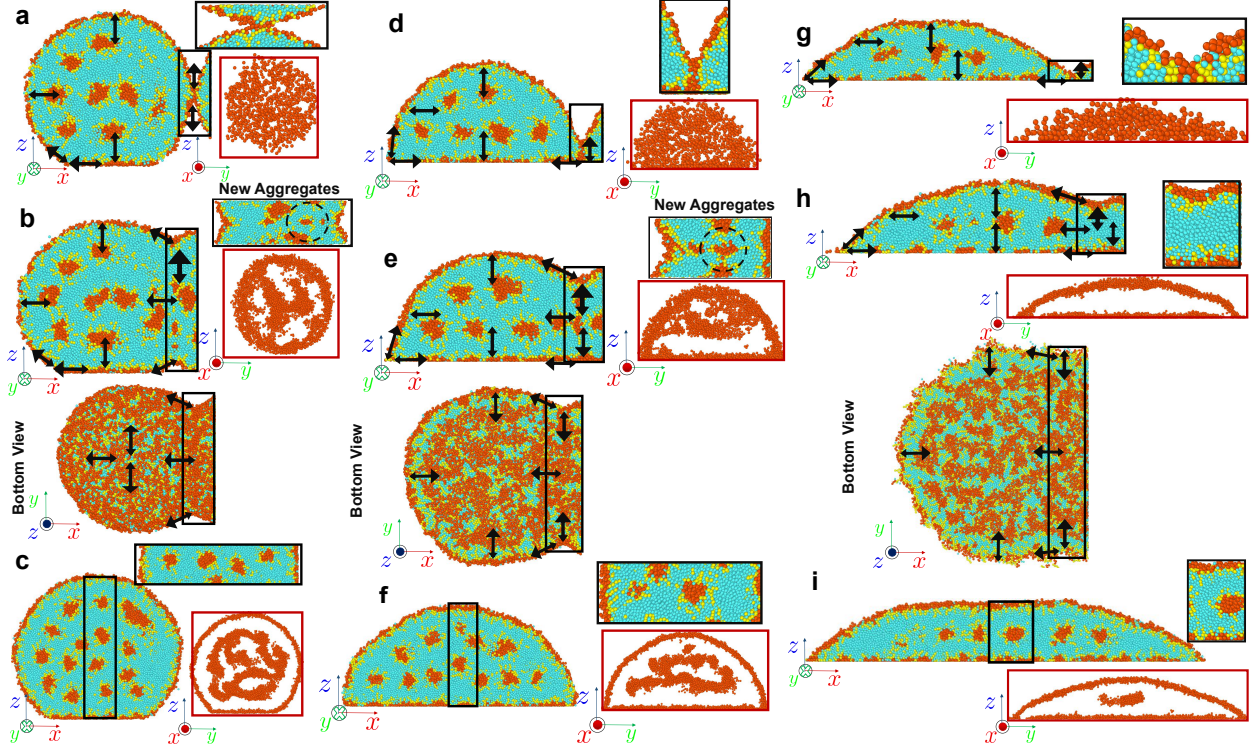


FIG. 5. Snapshots of coalescing droplets with C10E4 surfactant and surfactant mass transport on substrates of different wettability. The surfactant concentration in the liquid phase is above CAC, namely 35.48 wt%. The size of the arrow heads reflects the probabilities associated with surfactant transport to the different droplet areas (see Table S5 of the SM for further details). (a–c) corresponds to the case  $\theta_s \simeq 142^\circ$  with snapshots obtained at times (a)  $t_c + 17.5 \tau$ , (b)  $t_c + 185.0 \tau$ , and (c)  $t_c + 1733.7 \tau$ . (d–f)  $\theta_s \simeq 94^\circ$ , with snapshots shown at times (d)  $t_c + 28.75 \tau$ , (e)  $t_c + 315.0 \tau$ , and (f)  $t_c + 1415.0 \tau$ . (g–i)  $\theta_s \simeq 49^\circ$  with snapshots at times (g)  $t_c + 200.0 \tau$ , (h)  $t_c + 1358.7 \tau$ , and (i)  $t_c + 2200.0 \tau$ . Snapshots in (a), (d), and (g) are soon after the end of the thermal regime. Snapshots (b) and (e) illustrate a clearly developed bridge with new aggregates formed in its bulk or additional monomers remaining at the bridge region. (h) shows a clearly developed bridge highlighting the absence of aggregates in the case  $\theta_s < 90^\circ$ . (c), (f), and (i) correspond to cases of a fully developed bridge. Magnified views of the bridge region and its cross-section (showing only surfactant hydrophobic beads in the bridge region, red) are attached above and to the right of the snapshots, respectively. Snapshots were obtained using Ovito software.<sup>79</sup>

substrates, a large portion of the surfaces of the two droplets come into contact forming a film. This major contact area difference may also explain the higher degree of participation of water molecules in the pinching process in the case of wettable substrates. Secondly, there is much less

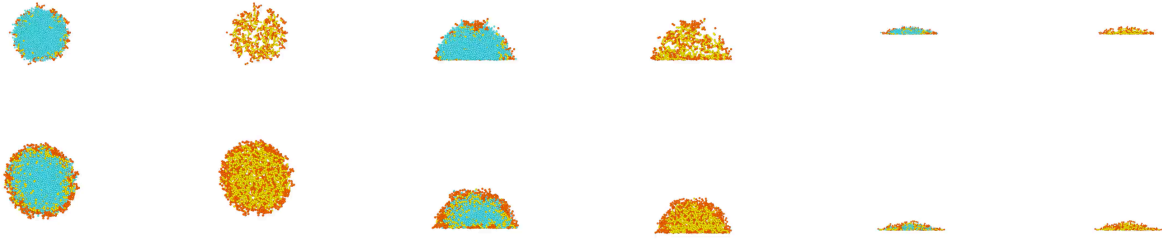


FIG. 6. (Multimedia view) Cross-section of the bridge during coalescence on different substrates (first two columns,  $\theta_s > 90^\circ$ , middle two columns,  $\theta_s \approx 90^\circ$ , and last two columns,  $\theta_s < 90^\circ$ ). Upper row shows the case of droplets with concentration lower than CAC (6.25 wt%), while the lower row with concentration above CAC (35.248 wt%). All beads (odd columns) or surfactant beads only (even columns) are shown at each cross-section at the bridge.

space in the bridge to form aggregates from any excess of surfactant that does not start at the bridge's LG surface. Finally, we note that surfactant transport from the contact line towards the SL and LG interface, is overall more pronounced than in the case of non-wettable substrates. This might be due to the immediate start of the decrease of the contact-line length as the droplets merge, resulting in a greater excess of surfactant in the contact-line region, and a greater migration to the LG and SL interfaces.

## B. Bridge dynamics

In the case  $\theta_s > 90^\circ$ , the pinching of the two droplets takes place well above the substrate (Figure 1b), and only later does the bridge region make contact with the substrate (Figure 1c). In the case  $\theta_s \leq 90^\circ$ , the bridge starts to form on the substrate from the onset of the coalescence process, which affects the bridge dynamics. The rate of coalescence can generally be described by the pace of the bridge growth in the direction normal as well as parallel to the substrate. The size of the bridge in these directions is  $b$  and  $w$ , respectively, both defined as shown in Figure 1. Figure 7 plots  $b$  and  $w$  above the CAC as a function of time (see Figures S3 and S4 in the SM for pure water and concentration below CAC.) In the cases above CAC and for nonwettable substrates ( $\theta_s > 90^\circ$ ), exponents for  $b$  are about 0.5, which are in line with the case of freely suspended droplets.<sup>83,84</sup> In contrast, in the case of wettable substrates, the exponent is higher reaching values of about 0.72, which suggests a much faster dynamics in comparison with the nonwettable substrates. Similarly,

the parameter  $w$  shows a similar but weaker tendency for growth with exponents of about 0.5 for both freely suspended droplets<sup>83,84</sup> and droplets on nonwetable substrates, up to about 0.65 for the wettable case. These higher values are agreeable with the  $2/3$  values seen for polymer droplets on wettable substrates.<sup>34</sup> In the case of water droplets, as a sanity check, exponents of  $b$  as well as  $w$  for both wettable and nonwettable substrates are in the range 0.60–0.66, which is in line with results reported in the literature,<sup>86</sup> where a power law of  $2/3$  has been suggested (see Figure S3a of the SM).

When surfactant concentration is below the CAC (Figure S3b of the SM), exponents for  $b$  are in the range 0.57–0.60 for non-wettable substrates (similar to pure water), but a significant increase of the exponent is noted for substrates reaching about 0.87, when the equilibrium contact angle of the droplet is about  $52^\circ$ . The exponents for  $w$  are in the range 0.55–0.68, with the highest exponents observed in the case of equilibrium contact angles close to  $70^\circ$ .

Finally, the initial thermal regime is well visible for sessile droplets as in the case of freely suspended droplets<sup>83,84</sup> or sessile polymer droplets.<sup>34</sup> However, we notice both a decreasing extent

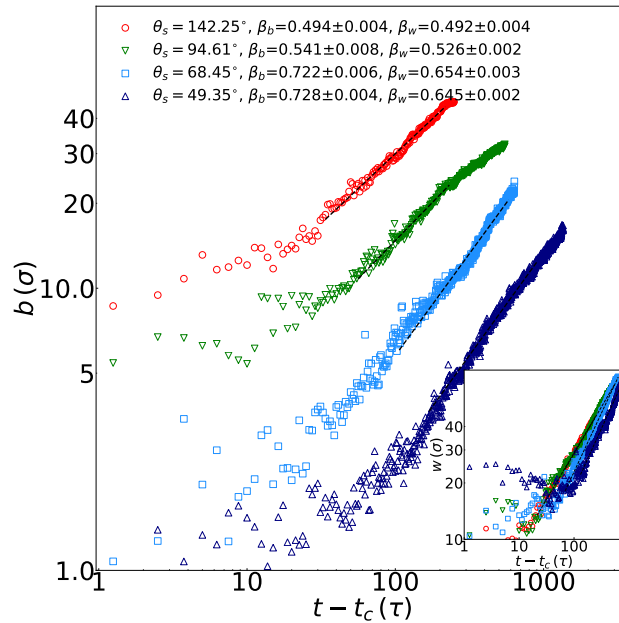


FIG. 7. Bridge height,  $b$ , as a function of time,  $t$ , starting from the pinching moment,  $t_c$ . Inset shows the bridge width,  $w$ . Results for droplets with surfactant concentration 35.48 wt% on substrates with different wettability, as indicated. The values of the power-law exponents for  $b$  and  $w$  are  $\beta_b$  and  $\beta_w$ , respectively, and are reported in the plot. Additional data for droplets without surfactant and with surfactant concentrations below CAC are reported in Figures S3 and S4 of the SM.

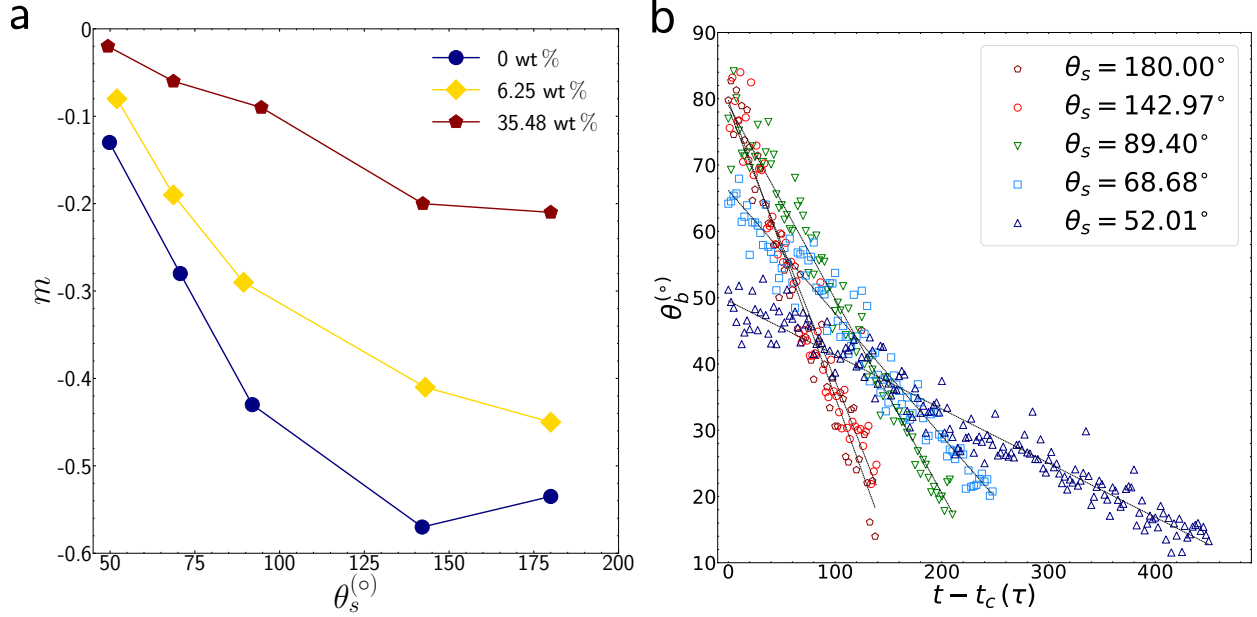


FIG. 8. (a) Rate of change of angle  $\theta_b$ ,  $m = d\theta_b/d(t - t_c)$ , as a function of the equilibrium contact angle,  $\theta_s$ , that expresses the wettability of the substrates with  $\theta_s > 90^\circ$  reflecting non-wettable cases.  $m$  is calculated from linear fits to the data of Figures S5 and S6 of the SM, where a linear change of  $\theta_b$  with time is observed to a good approximation. The  $\theta_s = 180^\circ$  data is for freely suspended droplets (no substrate). As an example here, panel b shows data for droplets with surfactant concentration 6.26 wt%.

of these fluctuations (smaller  $b$ ,  $w$ ) for sessile droplets when  $\theta_s < 90^\circ$ , due to the additional attraction and the contact with the substrate which suppresses these fluctuations, but also concurrently a strong lengthening of this regime in time, by almost an order of magnitude.

### C. Angle formed at the bridge

We monitored the angle  $\theta_b$  (Figure 1) as a function of time for all cases by employing the method of Ref. 96 (see Figure S1 and text in the SM). In particular, a layer parallel to the substrate at a distance  $b$  was considered, as indicated by the dashed line of Figure 1g. The dimensions of the spherical-cap liquid-phase above this layer were recorded in the  $x$  and  $y$  directions, as well as the distance of the apex from the layer, which are used as input to calculate  $\theta_b$ .<sup>96</sup> The approach has been applied in both the right and the left parts of the merged droplets and the average was taken, resulting in the final values reported for  $\theta_b$ . Time traces of  $\theta_b$  are plotted in Figures S5 and S6 of the SM for all cases considered here, while an example is shown in Figure 8. We can



observe that  $\theta_b$  exhibits to a large degree a linear behavior with time, which allows us to gather the slopes of the various curves and thus monitor the rate of change (dynamics) of this angle,  $m$ , during coalescence.

These rates of change data are plotted in Figure 8. The rate slows down as the substrate becomes more wettable, whether surfactant is present or not, but for  $\theta_s \gtrsim 140^\circ$ , the freely suspended behavior is already reached. This is also directly seen in Figure S5 of the SM. Greater surfactant concentration also slows down the process, as could be suspected from the earlier suspended droplet studies<sup>83,84</sup>, with pure water droplets being the fastest. Hence, the use of surfactant facilitates the smoothing of the wedge formation at the bridge apex.

#### D. Velocity of approach

We calculated the coalescing system length,  $X$ , as defined in Figure 1, and done in our previous work in the context of sessile polymer droplets.<sup>34</sup> Its value is approximately one droplet diameter.

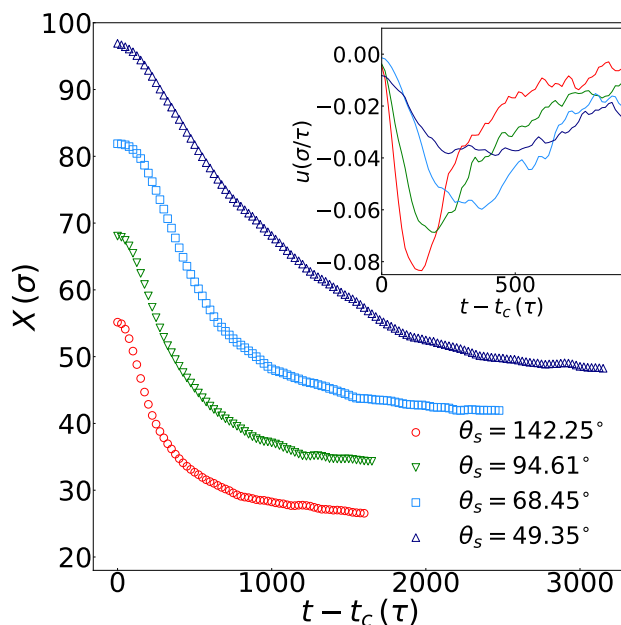


FIG. 9. The distance between the centers of mass of the two droplets in the  $x$ -direction,  $X$ , (see Figure 1) as a function of time,  $t$ , starting from the moment of first contact of the droplets,  $t_c$ , for surfactant-laden droplets of concentrations above CAC (35.48 wt%). The inset shows the instantaneous velocity,  $u = \dot{X}$ . Data for water droplets and surfactant-laden droplets with concentration below CAC are shown in Figure S7 of the SM.



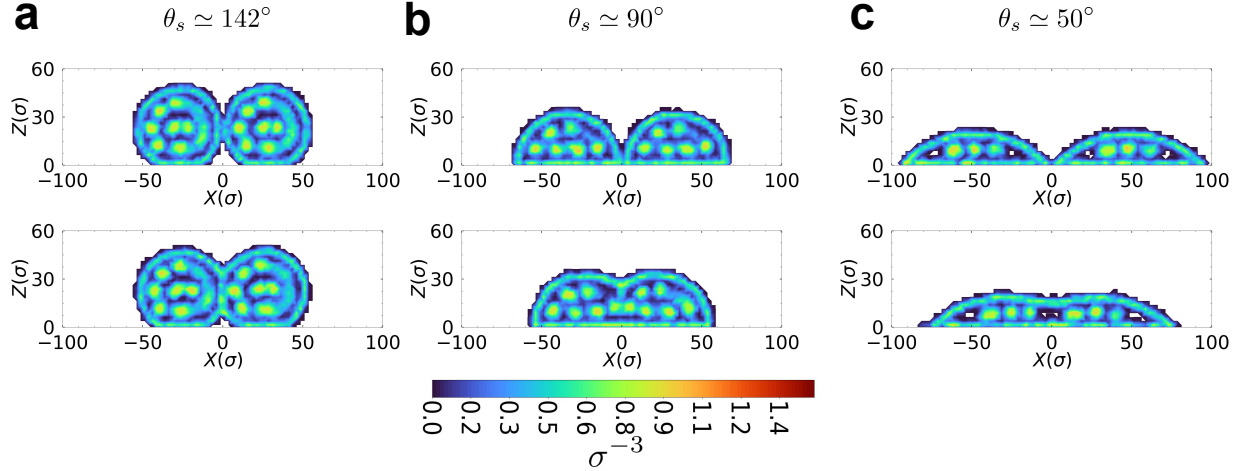


FIG. 10. Surfactant density at the moment of pinching (upper panels) and at a time when the bridge has been clearly developed (bottom panels) for above droplets with surfactant concentration amounting to 35.48 wt%. Here, cases for substrates with different wettability are shown, namely, (a)  $\theta_s \simeq 142^\circ$ , snapshots taken at  $t_c$  and  $t_c + 100 \tau$ , (b)  $\theta_s \simeq 90^\circ$ , snapshots taken at  $t_c$  and  $t_c + 412.5 \tau$ , and (c)  $\theta_s \simeq 50^\circ$ , snapshots taken at  $t_c$  and  $t_c + 1352.5 \tau$ .

Its time derivative,  $u = \dot{X}$ , provides a measure of how fast the droplets approach each other. Figure 9 presents  $X$  for droplets above the CAC on various substrates with different wettability, while data for water droplets and droplets with surfactant with a concentration below CAC are given in Figure S7 of the SM. Overall, the velocity of approach is smaller in the case of wettable substrates, irrespective of surfactant concentration, paralleling what we saw with bridge sizes  $b$  and  $w$  and the angle formed at the bridge  $\theta_b$ . This is also true for water droplets. The plots of Figure S8 of the SM show that an increase of surfactant concentration also significantly slows down the approach of the two droplets. This is mostly noticeable in the case of high concentrations, while surfactant-laden droplets with concentration below CAC show a similar behavior to pure water. Moreover, surfactant smooths the approach of the two droplets, as can be seen by the change of shape of the velocity of approach curves, particularly visible in Figure S8 of the SM. Finally, there is a clear shift in the moment of maximum velocity to later times for more wettable substrates at higher surfactant concentration, though this shift is much smaller in the latter case.

## E. Density Profiles

The density of surfactant molecules on a cross-section parallel to the  $x - z$  plane and passing through the center of mass of the droplets is presented in Figure 10. Also, Figure S9 of the SM shows the corresponding density distribution of water molecules for various substrates. We observe the formation of surfactant aggregates during the coalescence for substrates with equilibrium contact angles larger than  $90^\circ$ , while it is absent for wettable substrates (see for example Fig. 5a–b and d–e versus g–h). Large concentrations of surfactant are distributed at the LG and SL interfaces. Interior to this lies an inner layer devoid of aggregates, which is particularly wide for the wettable droplets. Notably the wettable case has a much smaller number of aggregates, despite the fact that all cases shown have the same concentration. This is due to the larger area of the LG and SL interfaces on wettable substrates, which might suggest that the CAC has a higher value. The smaller thickness of the wettable droplets, also, hinders the accommodation of a larger number of surfactant aggregates.

## IV. CONCLUSIONS

In this study, we have investigated the coalescence of sessile surfactant-laden droplets on substrates with different wettability, including those with equilibrium contact-angle higher as well as lower than  $90^\circ$ . We have explored the influence of surfactant concentration both below and above the CAC, and we juxtaposed our results with the case of pure water droplets. In particular, we have elucidated the mass transport mechanism in all these cases and explored the dynamics of the coalescence process by following the height and width of the bridge, the rate of change of the bridge angle, as well as the velocity of approach of the droplets.

Overall, sessile droplets with  $\theta_s \geq 90^\circ$  share similarities with freely suspended droplets, and for  $\theta_s \simeq 140^\circ$  already behave practically identically as if they were freely suspended. In this case, the influence of the substrate on the coalescence process is rather small. For example, the pinching region is mainly driven by the interaction of the surfactant molecules at the droplets' LG surface, as in the case of the freely suspended droplets. In contrast, in the case of wettable substrates ( $\theta_s < 90^\circ$ ), we see that water molecules are part of the pinching process, a significant departure from the physics of the freely suspended case. The mass transport of surfactant molecules during coalescence also shows some differences between wettable and nonwetable substrates, which

mostly relates to their intensity. A more notable difference is the absence of newly formed aggregates as the bridge grows during coalescence in the case of wettable substrates. This is due to the lower amount of surfactant at the pinching region as the initial contact film has a far smaller area. In fact, the nature of the surface of first contact changes dramatically from a circular region to a thin contact line when the threshold of contact angle  $\theta_s \approx 90^\circ$  is crossed. The smaller amount of space available in the bridge region between the LG and SL interfaces during later evolution also contributes. The latter is related to a still open question of identifying changes in CAC when the equilibrium contact angle of the droplets changes.

We also found that an increased wettability of the substrate leads to higher rate exponents for the growth of the bridge radius,  $b$ , and its width,  $w$ , but generally exponents for  $w$  are lower. We confirm the approach to a  $\approx \frac{2}{3}$  rate exponent at low contact angles suggested by several previous studies,<sup>34,86</sup> but see no evidence for the previously proposed linear growth.<sup>81</sup> Overall, surfactant will decelerate the coalescence of the sessile droplets, when above CAC, but we observed higher exponents in the case of concentration below the CAC for wettable substrates, which is not fully understood at the moment. Similarly, the bridge angle,  $\theta_b$ , changes at a faster pace in the case of water droplets and low concentration and when the wettability of the substrate is lower (larger  $\theta_s$ ). Finally, by analyzing the velocity of approach of the two droplets, which is generally high at the initial stages of coalescence when the bridge forms, we found that more wettable substrates and a higher surfactant concentration will lead to smoother changes in the velocity, less acceleration. We anticipate that our study provides fundamental insights into the coalescence of sessile surfactant-laden droplets, an important phenomenon that has previously mostly remained unexplored at the molecular-scale level.

## V. SUPPLEMENTARY MATERIAL

The SM contains: details on the estimation of the contact angle of a sessile droplet. Calibration of the dependence of the contact angle of a water droplet as a function of the droplet–substrate attraction parameter  $\epsilon_{ws}$ . Table of the water–substrate and surfactant–substrate interaction parameters. Further data and methodology details on the mass transport mechanism along with the probabilities of surfactant moving between different areas of the droplets. Data on the bridge angle, the velocity of approach, and the density profiles of the droplets, for a wider set of parameters than shown in the main text.

## ACKNOWLEDGMENTS

This research has been supported by the National Science Centre, Poland, under grant No. 2019/34/E/ST3/00232. We gratefully acknowledge Polish high-performance computing infrastructure PLGrid (HPC Centers: ACK Cyfronet AGH) for providing computer facilities and support within computational grant no. PLG/2022/015747.

## REFERENCES

- <sup>1</sup>J. D. Paulsen, R. Carmigniani, A. Kannan, J. C. Burton, and S. R. Nagel, “Coalescence of bubbles and drops in an outer fluid,” *Nat. Commun.* **5**, 3182 (2014).
- <sup>2</sup>Y. Yoon, F. Baldessari, H. D. Ceniceros, and L. G. Leal, “Coalescence of two equal-sized deformable drops in an axisymmetric flow,” *Phys. Fluids* **19**, 102102 (2007).
- <sup>3</sup>M. I. Khodabocus, M. Sellier, and V. Nock, “Scaling laws of droplet coalescence: Theory and numerical simulation,” *Adv. Math. Phys.* **2018**, 4906016 (2018).
- <sup>4</sup>S. Perumanath, M. K. Borg, M. V. Chubynsky, J. E. Sprittles, and J. M. Reese, “Droplet coalescence is initiated by thermal motion,” *Phys. Rev. Lett.* **122**, 104501 (2019).
- <sup>5</sup>J. Eggers, J. R. Lister, and H. A. Stone, “Coalescence of liquid drops,” *J. Fluid Mech.* **401**, 293–310 (1999).
- <sup>6</sup>D. G. Aarts, H. N. Lekkerkerker, H. Guo, G. H. Wegdam, and D. Bonn, “Hydrodynamics of droplet coalescence,” *Phys. Rev. Lett.* **95**, 164503 (2005).
- <sup>7</sup>J. E. Sprittles and Shikhmurzaev, “Coalescence of liquid drops: Different models versus experiment,” *Phys. Fluids* **24**, 122105 (2012).
- <sup>8</sup>M. Dudek, D. Fernandes, E. Helno Herø, and G. Øye, “Microfluidic method for determining drop-drop coalescence and contact times in flow,” *Colloids Surf. A: Physicochem. Eng. Asp.* **586**, 124265 (2020).
- <sup>9</sup>M. M. Rahman, W. Lee, A. Iyer, and S. J. Williams, “Viscous resistance in drop coalescence,” *Phys. Fluids* **31**, 012104 (2019).
- <sup>10</sup>J. D. Berry and R. R. Dagastine, “Mapping coalescence of micron-sized drops and bubbles,” *J. Colloid Interface Sci.* **487**, 513–522 (2017).
- <sup>11</sup>P. M. Somwanshi, K. Muralidhar, and S. Khandekar, “Coalescence dynamics of sessile and pendant liquid drops placed on a hydrophobic surface,” *Phys. Fluids* **30**, 092103 (2018).

- <sup>12</sup>P. K. Kirar, K. Alvarenga, P. Kolhe, G. Biswas, and K. Chandra Sahu, “Coalescence of drops on the free-surface of a liquid pool at elevated temperatures,” *Phys. Fluids* **32**, 052103 (2020).
- <sup>13</sup>S. Bayani, Y. Tabe, Y. T. Kang, S. H. Lee, and C. K. Choi, “Surface plasmon resonance imaging of drop coalescence at high-temporal resolution,” *J. Flow Vis. Image Process.* **25**, 191–205 (2018).
- <sup>14</sup>M. Brik, S. Harmand, and I. Zaaroura, “Relaxation and contact angle dynamics during the coalescence of different sized vertically aligned water drops in different silicone oil viscosities,” *Colloids Surf. A: Physicochem. Eng. Asp.* **629**, 127429 (2021).
- <sup>15</sup>C. R. Anthony, M. T. Harris, and O. A. Basaran, “Initial regime of drop coalescence,” *Phys. Rev. Fluids* **5**, 033608 (2020).
- <sup>16</sup>V. R. Kern, T. Sæter, and A. Carlson, “Viscoplastic sessile drop coalescence,” *Phys. Rev. Fluids* **7**, L081601 (2022).
- <sup>17</sup>M. Heinen, M. Hoffmann, F. Diewald, S. Seckler, K. Langenbach, and J. Vrabec, “Droplet coalescence by molecular dynamics and phase-field modeling,” *Phys. Fluids* **34**, 042006 (2022).
- <sup>18</sup>M. Geri, B. Keshavarz, G. H. McKinley, and J. W. M. Bush, “Thermal delay of drop coalescence,” *J. Fluid Mech.* **833**, R3 (2017).
- <sup>19</sup>M. Abouelsoud and B. Bai, “Bouncing and coalescence dynamics during the impact of a falling drop with a sessile drop on different solid surfaces,” *Phys. Fluids* **33**, 063309 (2021).
- <sup>20</sup>L. Hilaire, B. Siboulet, S. Charton, and J.-F. Dufrière, “Coalescence initiation in liquid–liquid systems: A stochastic model,” *Langmuir* **39**, 14853–14858 (2023).
- <sup>21</sup>E. G. Bowen, “The formation of rain by coalescence,” *Aust. J. Chem.* **3**, 193–213 (1950).
- <sup>22</sup>M. Denys, P. Deuar, Z. Che, and P. E. Theodorakis, “A lagrangian particle-based numerical model for surfactant-laden droplets at macroscales,” *Phys. Fluids* **34**, 095126 (2022).
- <sup>23</sup>E. X. Berry and R. L. Reinhardt, “An analysis of cloud drop growth by collection: part 3. accretion and self-collection,” *J. Atmos. Sci.* **31**, 2118–2126 (1974).
- <sup>24</sup>A. Kovetz and B. Olund, “The effect of coalescence and condensation on rain formation in a cloud of finite vertical extent,” *J. Atmos. Sci.* **26**, 1060–1065 (1969).
- <sup>25</sup>M. Singh, H. Haverinen, P. Dhagat, and G. Jabbour, “Inkjet printing process and its applications,” *Adv. Mater.* **22**, 673–685 (2010).
- <sup>26</sup>S. Feng, L. Yi, L. Zhao-Miao, C. Ren-Tuo, and W. Gui-Ren, “Advances in micro-droplets coalescence using microfluidics,” *Chinese J. Anal. Chem.* **43**, 1942–1954 (2015).

- <sup>27</sup>M. Dudek, J. Chicault, and G. Øye, “Microfluidic investigation of crude oil droplet coalescence: effect of oil/water composition and droplet aging,” *Energy Fuels* **34**, 5110–5120 (2019).
- <sup>28</sup>K. Choi, A. H. Ng, R. Fobel, and A. R. Wheeler, “Digital microfluidics,” *Annu. Rev. Anal. Chem.* **5**, 413–440 (2012).
- <sup>29</sup>R. B. Fair, “Digital microfluidics: is a true lab-on-a-chip possible?” *Microfluid. Nanofluid.* **3**, 245–281 (2007).
- <sup>30</sup>T. Thomas and H. N. Unni, “Led-based opto-wetting and fluidic transport for droplet mixing,” *Microfluid. Nanofluid.* **23**, 1–12 (2019).
- <sup>31</sup>H. Wijshoff, “The dynamics of the piezo inkjet printhead operation,” *Phys. Rep.* **491**, 77–177 (2010).
- <sup>32</sup>P. J. Dekker, M. A. Hack, W. Tewes, C. Datt, A. Bouillant, and J. H. Snoeijer, “When elasticity affects drop coalescence,” *Phys. Rev. Lett.* **128**, 028004 (2022).
- <sup>33</sup>E. Calvo, E. de Malmazet, F. Risso, and O. Masbernat, “Coalescence of water drops at an oil–water interface loaded with microparticles and surfactants,” *Ind. Eng. Chem. Res.* **58**, 15573–15587 (2019).
- <sup>34</sup>S. Arbabi and P. E. Theodorakis, “Coalescence of sessile polymer droplets: A molecular dynamics study,” *Macromol. Theory Simul.* , 2300017 (2023).
- <sup>35</sup>S. C. Varma, A. Saha, and A. Kumar, “Coalescence of polymeric sessile drops on a partially wettable substrate,” *Phys. Fluids* **33**, 123101 (2021).
- <sup>36</sup>V. S. Sivasankar, S. A. Etha, D. R. Hines, and S. Das, “Coalescence of microscopic polymeric drops: Effect of drop impact velocities,” *Langmuir* **37**, 13512–13526 (2021).
- <sup>37</sup>V. S. Sivasankar, D. R. Hines, and S. Das, “Numerical study of the coalescence and mixing of drops of different polymeric materials,” *Langmuir* **38**, 14084–14096 (2022).
- <sup>38</sup>M. R. Otazo, R. Ward, G. Gillies, R. S. Osborne, M. Golding, and M. A. K. Williams, “Aggregation and coalescence of partially crystalline emulsion drops investigated using optical tweezers,” *Soft Matter* **15**, 6383–6391 (2019).
- <sup>39</sup>C. Vannozzi, “Effect of polymer-coated gold nanoparticle stabilizers on drop coalescence,” *Phys. Fluids* **31**, 082112 (2019).
- <sup>40</sup>N. I. Politova, S. Tcholakova, S. Tsibranska, N. D. Denkov, and K. Muelheims, “Coalescence stability of water-in-oil drops: Effects of drop size and surfactant concentration,” *Colloids Surf. A: Physicochem. Eng. Asp.* **531**, 32–39 (2017).

- <sup>41</sup>W. H. Weheliye, T. Dong, and P. Angeli, “On the effect of surfactants on drop coalescence at liquid/liquid interfaces,” *Chem. Eng. Sci.* **161**, 215–227 (2017).
- <sup>42</sup>G. Soligo, A. Roccon, and A. Soldati, “Coalescence of surfactant-laden drops by phase field method,” *J. Comput. Phys.* **376**, 1292–1311 (2019).
- <sup>43</sup>T. Dong, W. H. Weheliye, P. Chausset, and P. Angeli, “An experimental study on the drop/interface partial coalescence with surfactants,” *Phys. Fluids* **29**, 102101 (2017).
- <sup>44</sup>T. Dong, W. H. Weheliye, and P. Angeli, “Laser induced fluorescence studies on the distribution of surfactants during drop/interface coalescence,” *Phys. Fluids* **31**, 012106 (2019).
- <sup>45</sup>N. M. Kovalchuk, M. Reichow, T. Frommweiler, D. Vigolo, and M. J. H. Simmons, “Mass transfer accompanying coalescence of surfactant-laden and surfactant-free drop in a microfluidic channel,” *Langmuir* **35**, 9184–9193 (2019).
- <sup>46</sup>T. C. Botti, A. Hutin, E. Quintella, and M. S. Carvalho, “Effect of interfacial rheology on drop coalescence in water–oil emulsion,” *Soft Matter* **18**, 1423–1434 (2022).
- <sup>47</sup>C. Constante-Amores, A. Batchvarov, L. Kahouadji, S. Shin, J. Chergui, D. Juric, and O. Matar, “Role of surfactant-induced marangoni stresses in drop-interface coalescence,” *J. Fluid Mech.* **925**, A15 (2021).
- <sup>48</sup>M. Kasmaee, F. Varaminian, P. Khadiv-Parsi, and J. Saien, “Effects of different surfactants and physical properties on the coalescence of dimethyl disulfide drops with mother phase at the interface of sodium hydroxide aqueous solutions,” *J. Mol. Liq.* **263**, 31–39 (2018).
- <sup>49</sup>E. Nowak, Z. Xie, N. M. Kovalchuk, O. K. Matar, and M. J. Simmons, “Bulk advection and interfacial flows in the binary coalescence of surfactant-laden and surfactant-free drops,” *Soft Matter* **13**, 4616–4628 (2017).
- <sup>50</sup>E. Nowak, N. M. Kovalchuk, Z. Che, and M. J. Simmons, “Effect of surfactant concentration and viscosity of outer phase during the coalescence of a surfactant-laden drop with a surfactant-free drop,” *Colloids Surf. A Physicochem. Eng. Asp.* **505**, 124–131 (2016).
- <sup>51</sup>N. Jaansson and J. Vermant, “Tensiometry and rheology of complex interfaces,” *Curr. Opin. Colloid Interface Sci.* **37**, 136–150 (2018).
- <sup>52</sup>S. Narayan, A. E. Metaxa, R. Bachnak, T. Neumiller, C. S. Dutcher, *et al.*, “Zooming in on the role of surfactants in droplet coalescence at the macro-and microscale,” *Curr. Opin. Colloid Interface Sci.* **50**, 101385 (2020).
- <sup>53</sup>I. B. Ivanov, K. D. Danov, and P. A. Kralchevsky, “Flocculation and coalescence of micron-size emulsion droplets,” *Colloids Surf. A Physicochem. Eng.* **152**, 161–182 (1999).

- <sup>54</sup>S. Tcholakova, N. D. Denkov, and T. Danner, “Role of surfactant type and concentration for the mean drop size during emulsification in turbulent flow,” *Langmuir* **20**, 7444–7458 (2004).
- <sup>55</sup>D. Langevin, “Coalescence in foams and emulsions: Similarities and differences,” *Curr. Opin. Colloid Interface Sci.* **44**, 23–31 (2019).
- <sup>56</sup>J. Lu and C. M. Corvalan, “Coalescence of viscous drops with surfactants,” *Chem. Eng. Sci.* **78**, 9–13 (2012).
- <sup>57</sup>O. D. Velev, T. D. Gurkov, and R. P. Borwankar, “Spontaneous cyclic dimpling in emulsion films due to surfactant mass transfer between the phases,” *J. Colloid Interface Sci.* **159**, 497–501 (1993).
- <sup>58</sup>V. C. Suja, A. Kar, W. Cates, S. M. Remmert, P. D. Savage, and G. G. Fuller, “Evaporation-induced foam stabilization in lubricating oils,” *Proc. Natl. Acad. Sci. U.S.A.* **115**, 7919–7924 (2018).
- <sup>59</sup>J.-C. Baret, “Surfactants in droplet-based microfluidics,” *Lab Chip*. **12**, 422–433 (2012).
- <sup>60</sup>K. S. Elvira, F. Gielen, S. S. Tsai, and A. M. Nightingale, “Materials and methods for droplet microfluidic device fabrication,” *Lab Chip*. **22**, 859–875 (2022).
- <sup>61</sup>R. W. Hopper, “Coalescence of two viscous cylinders by capillarity: Part i, theory,” *J. Am. Ceram. Soc* **76**, 2947–2952 (1993).
- <sup>62</sup>M. A. Bruning, M. Costalonga, S. Karpitschka, and J. H. Snoeijer, “Delayed coalescence of surfactant containing sessile droplets,” *Phys. Rev. Fluids* **3**, 073605 (2018).
- <sup>63</sup>H. Yi, T. Fu, C. Zhu, and Y. Ma, “Cascade coalescence of droplets in a sudden expansion microchannel,” *Chem. Eng. J.* **442**, 136240 (2022).
- <sup>64</sup>A. Schwarzwälder, J. Meyer, and A. Dittler, “Experimental analysis of droplet coalescence and transport mechanisms on a single vertical fiber,” *Exp. Fluids* **64**, 103 (2023).
- <sup>65</sup>Y. Sun, D. Yang, H. Sun, H. Wu, Q. Chang, L. Shi, Y. Cao, Y. He, and T. Xie, “Experimental study on the falling and coalescence characteristics of droplets under alternating electric fields,” *Colloids Surf. A Physicochem. Eng. Asp.* **603**, 125136 (2020).
- <sup>66</sup>M. W. Lee, D. K. Kang, S. S. Yoon, and A. L. Yarin, “Coalescence of two drops on partially wettable substrates,” *Langmuir* **28**, 3791–3798 (2012).
- <sup>67</sup>S. Chen, J. Wang, C. Chen, and A. Mahmood, “Understanding the coalescence and non-coalescence of underwater oil droplets,” *Chem. Phys.* **529**, 110466 (2020).



- <sup>68</sup>C. J. Park, J. Ha, J. H. Lee, and H.-Y. Kim, “Coalescence of oil drops and films on micropillared substrates enabled by enhanced water drainage through pillar gaps,” *Soft Matter* **17**, 5888–5896 (2021).
- <sup>69</sup>L. Duchemin, J. Eggers, and C. Josserand, “Inviscid coalescence of drops,” *J. Fluid Mech.* **487**, 167–178 (2003).
- <sup>70</sup>L. Leal, “Flow induced coalescence of drops in a viscous fluid,” *Phys. Fluids* **16**, 1833–1851 (2004).
- <sup>71</sup>M. Chinaud, V. Voulgaropoulos, and P. Angeli, “Surfactant effects on the coalescence of a drop in a hele-shaw cell,” *Phys. Rev. E* **94**, 033101 (2016).
- <sup>72</sup>J. Shaikh, N. D. Patil, A. Sharma, and R. Bhardwaj, “Numerical simulations and experiments on droplet coalescence dynamics over a liquid–air interface: Mechanism and effect of droplet-size/surface-tension,” *SN Appl. Sci.* **3**, 292 (2021).
- <sup>73</sup>K. Gu, T. Gang, and L. Chen, “Numerical simulation of droplet coalescence based on the sph method,” *Theor. Appl. Mech. Lett.* **12**, 100333 (2022).
- <sup>74</sup>L. Y. Yeo, O. K. Matar, E. S. P. de Ortiz, and G. F. Hewitt, “Film drainage between two surfactant-coated drops colliding at constant approach velocity,” *J. Colloid Interface Sci.* **257**, 93–107 (2003).
- <sup>75</sup>Y. Hu, D. Pine, and L. G. Leal, “Drop deformation, breakup, and coalescence with compatibilizer,” *Phys. Fluids* **12**, 484–489 (2000).
- <sup>76</sup>A. Mansouri, H. Arabnejad, and R. Mohan, “Numerical investigation of droplet-droplet coalescence and droplet-interface coalescence,” in *FEDSM*, Vol. 46216 (American Society of Mechanical Engineers, 2014) p. V01AT05A006.
- <sup>77</sup>J.-Y. Chen, P. Gao, Y.-T. Xia, E.-Q. Li, H.-R. Liu, and H. Ding, “Early stage of delayed coalescence of soluble paired droplets: A numerical study,” *Phys. Fluids* **33**, 092005 (2021).
- <sup>78</sup>F. Y. Leong and D.-V. Le, “Droplet dynamics on viscoelastic soft substrate: Toward coalescence control,” *Phys. Fluids* **32**, 062102 (2020).
- <sup>79</sup>A. Stukowski, “Visualization and analysis of atomistic simulation data with ovito—the open visualization tool,” *Model. Simul. Mater. Sci. Eng.* **18**, 015012 (2010).
- <sup>80</sup>C. Verdier and M. Brizard, “Understanding droplet coalescence and its use to estimate interfacial tension,” *Rheol. Acta* **41**, 514–523 (2002).
- <sup>81</sup>J. Hernández-Sánchez, L. Lubbers, A. Eddi, and J. Snoeijer, “Symmetric and asymmetric coalescence of drops on a substrate,” *Phys. Rev. Lett* **109**, 184502 (2012).

- <sup>82</sup>J. D. Paulsen, “Approach and coalescence of liquid drops in air,” *Phys. Rev. E* **88**, 063010 (2013).
- <sup>83</sup>S. Arbabi, P. Deuar, M. Denys, R. Bennacer, Z. Che, and P. E. Theodorakis, “Coalescence of surfactant-laden droplets,” *Phys. Fluids* **35**, 063329 (2023).
- <sup>84</sup>S. Arbabi, P. Deuar, M. Denys, R. Bennacer, Z. Che, and P. E. Theodorakis, “Molecular dynamics simulation of the coalescence of surfactant-laden droplets,” *Soft Matter* **19**, 8070–8080 (2023).
- <sup>85</sup>T. Li, “Molecular dynamics simulations of droplet coalescence and impact dynamics on the modified surfaces: A review,” *Comput. Mater. Sci.* **230**, 112547 (2023).
- <sup>86</sup>A. Eddi, K. Winkels, and J. Snoeijer, “Influence of droplet geometry on the coalescence of low viscosity drops,” *Phys. Rev. Lett.* **111**, 144502 (2013).
- <sup>87</sup>W. Ristenpart, P. McCalla, R. Roy, and H. Stone, “Coalescence of spreading droplets on a wettable substrate,” *Phys. Rev. Lett.* **97**, 064501 (2006).
- <sup>88</sup>R. Narhe, D. Beysens, and Y. Pomeau, “Dynamic drying in the early-stage coalescence of droplets sitting on a plate,” *EPL* **81**, 46002 (2008).
- <sup>89</sup>N. Kapur and P. H. Gaskell, “Morphology and dynamics of droplet coalescence on a surface,” *Phys. Rev. E* **75**, 056315 (2007).
- <sup>90</sup>P. Bazazi and S. H. Hejazi, “Retarding spreading of surfactant drops on solid surfaces: Interplay between the marangoni effect and capillary flows,” *Phys. Rev. Fluids* **5**, 084006 (2020).
- <sup>91</sup>P. Yatsyshin and S. Kalliadasis, “Surface nanodrops and nanobubbles: a classical density functional theory study,” *J. Fluid Mech.* **913**, A45 (2021).
- <sup>92</sup>S. C. Varma, A. Saha, S. Mukherjee, A. Bandopadhyay, A. Kumar, and S. Chakraborty, “Universality in coalescence of polymeric fluids,” *Soft Matter* **16**, 10921–10927 (2020).
- <sup>93</sup>S. C. Varma, D. Dasgupta, and A. Kumar, “Elasticity can affect droplet coalescence,” *Phys. Rev. Fluids* **34**, 028004 (2022).
- <sup>94</sup>C. Verdier, “Coalescence of polymer droplets: experiments on collision,” *C. R. Acad. Sci. Paris, Ser. IV, Phys.* **1**, 119–126 (2000).
- <sup>95</sup>P. E. Theodorakis, E. A. Müller, R. V. Craster, and O. K. Matar, “Superspreading: Mechanisms and molecular design,” *Langmuir* **31**, 2304–2309 (2015).
- <sup>96</sup>P. E. Theodorakis, E. A. Müller, R. V. Craster, and O. K. Matar, “Modelling the superspreading of surfactant-laden droplets with computer simulation,” *Soft Matter* **11**, 9254–9261 (2015).

- <sup>97</sup>P. E. Theodorakis, E. R. Smith, and Müller, “Spreading of aqueous droplets with common and superspreading surfactants. a molecular dynamics study,” *Colloids Surf. A: Physicochem. Eng. Aspects.* **581**, 123810 (2019).
- <sup>98</sup>O. Lobanova, C. Avendaño, T. Lafitte, E. A. Müller, and G. Jackson, “SAFT- $\gamma$  force field for the simulation of molecular fluids. 4. a single-site coarse-grained model of water applicable over a wide temperature range.” *Mol. Phys.* **113**, 1228–1249 (2015).
- <sup>99</sup>O. Lobanova, *Development of coarse-grained force fields from a molecular based equation of state for thermodynamic and structural properties of complex fluids*, Ph.D. thesis, Imperial College London (2014).
- <sup>100</sup>O. Lobanova, A. Mejia, G. Jackson, and E. A. Müller, “Saft- $\gamma$  force field for the simulation of molecular fluids 6: Binary and ternary mixtures comprising water, carbon dioxide, and n-alkanes,” *J. Chem. Thermodyn.* **93**, 320–336 (2016).
- <sup>101</sup>P. Morgado, O. Lobanova, E. A. Müller, G. Jackson, M. Almeida, and E. J. Filipe, “Saft- $\gamma$  force field for the simulation of molecular fluids: 8. hetero-segmented coarse-grained models of perfluoroalkylalkanes assessed with new vapour–liquid interfacial tension data,” *Mol. Phys.* **114**, 2597–2614 (2016).
- <sup>102</sup>E. A. Müller and G. Jackson, “Force field parameters from the SAFT- $\gamma$  equation of state for use in coarse-grained molecular simulations,” *Annu. Rev. Chem. Biomol. Eng.* **5**, 405–427 (2014).
- <sup>103</sup>T. Lafitte, A. Apostolakou, C. Avendaño, A. Galindo, C. S. Adjiman, E. A. Müller, and G. Jackson, “Accurate statistical associating fluid theory for chain molecules formed from mie segments,” *J. Chem. Phys.* **139**, 154504 (2013).
- <sup>104</sup>C. Avendaño, T. Lafitte, A. Galindo, C. S. Adjiman, G. Jackson, and E. A. Müller, “Saft- $\gamma$  force field for the simulation of molecular fluids. 1. a single-site coarse grained model of carbon dioxide,” *J. Phys. Chem B* **115**, 11154–11169 (2011).
- <sup>105</sup>C. Avendaño, T. Lafitte, A. Galindo, C. S. Adjiman, E. A. Müller, and G. Jackson, “Saft- $\gamma$  force field for the simulation of molecular fluids: 2. coarse-grained models of greenhouse gases,” *J. Phys. Chem B* **117**, 2717–2733 (2013).
- <sup>106</sup>S. Plimpton, “Fast parallel algorithms for short-range molecular dynamics,” *J. Comp. Phys.* **117**, 1–19 (1995).
- <sup>107</sup>A. P. Thompson, H. M. Aktulga, R. Berger, D. S. Bolintineanu, W. M. Brown, P. S. Crozier, P. J. in ’t Veld, A. Kohlmeyer, S. G. Moore, T. D. Nguyen, R. Shan, M. J. Stevens, J. Tranchida,

- C. Trott, and S. J. Plimpton, “LAMMPS - a flexible simulation tool for particle-based materials modeling at the atomic, meso, and continuum scales,” *Comp. Phys. Comm.* **271**, 108171 (2022).
- <sup>108</sup>P. E. Theodorakis, E. R. Smith, R. V. Craster, E. A. Müller, and O. K. Matar, “Molecular dynamics simulation of the superspreading of surfactant-laden droplets. a review,” *Fluids* **4**, 176 (2019).
- <sup>109</sup>P. E. Theodorakis, E. A. Müller, R. V. Craster, and O. K. Matar, “Insights into surfactant-assisted superspreading,” *Curr. Opin. Colloid Interface Sci.* **19**, 283–289 (2014).
- <sup>110</sup>J. Stillinger, Frank H., “Rigorous Basis of the Frenkel-Band Theory of Association Equilibrium,” *J. Chem. Phys* **38**, 1486–1494 (1963).
- <sup>111</sup>P. E. Theodorakis, W. Paul, and K. Binder, “Analysis of the cluster formation in two-component cylindrical bottle-brush polymers under poor solvent conditions. a simulation study,” *Eur. Phys. J. E* **34**, 52 (2011).
- <sup>112</sup>F. Mugele, T. Becker, R. Nikopoulos, M. Kohonen, and S. Herminghaus, “Capillarity at the nanoscale: an afm view,” *J. Adhes. Sci. Technol.* **16**, 951–964 (2002).